MASTER PLOT ANALYSIS OF MICROCRACKING IN GRAPHITE/EPOXY AND GRAPHITE/PEEK LAMINATES*

John A. Nairn, Shoufeng Hu, and Jong Song Bark
Material Science and Engineering, University of Utah
Salt Lake City, Utah 84112, USA

ABSTRACT

We used a variational stress analysis and an energy release rate failure criterion to construct a master plot analysis of matrix microcracking. In the master plot, the results for all laminates of a single material are predicted to fall on a single line whose slope gives the microcracking toughness of the material. Experimental results from 18 different layups of AS4/3501-6 laminates show that the master plot analysis can explain all observations. In particular, it can explain the differences between microcracking of central 90° plies and of free-surface 90° plies. Experimental results from two different AS4/PEEK laminates tested at different temperatures can be explained by a modified master plot that accounts for changes in the residual thermal stresses. Finally, we constructed similar master plot analyses for previous literature microcracking models. All microcracking theories that ignore the thickness dependence of the stresses gave poor results.

INTRODUCTION

When the 90° plies are relatively less stiff than the supporting plies, the first form of damage in $[(S)/90_n]_s$ or $[90_n/(S)]_s$ laminates (where (S) denotes any orthotropic sublaminate) is usually microcracking or transverse cracking of the 90° ply groups [1–16]. When the 90° plies are in the middle ($[(S)/90_n]_s$ laminates), those plies crack into an array of roughly periodic microcracks. When the 90° plies are on the outside ($[90_n/(S)]_s$ laminates), the 90° ply groups also crack into an array of roughly periodic microcracks, but the two arrays are shifted from each other by half the average crack spacing [10, 17]. There are many reasons for studying microcracking. Microcracks not only change the thermal and mechanical properties of laminates [10, 18], but also present pathways through which corrosive agents may penetrate into the interior of the laminate [6]. Perhaps most importantly, microcracks act as nuclei for further damage such as delamination [1, 9], longitudinal splitting [5, 6], and curved microcracks [15]. Because microcracks are precursors to the cascade of events that leads to laminate failure, we would have little hope of understanding laminate failure or of predicting long-term durability if we did not first develop a thorough understanding of the phenomenon of microcracking.

To predict microcracking results in $[(S)/90_n]_s$ laminates under uniform axial loading of σ_0, Nairn *et. al.* [16, 19] advocated an energy release rate failure criterion. In brief, the next microcrack is assumed to form when the total energy release rate associated with the formation of that microcrack, G_m, equals or exceeds the microcracking fracture toughness of the material, G_{mc}. From a thermoelastic, variational mechanics stress state [16, 19–21], the total energy release rate due to microcracking is [16, 19–21]

$$G_m = \sigma_{x0}^{(1)2} C_3 t_1 Y(D) \tag{1}$$

*Work supported, in part, by contract NAS1-18833 from NASA Langley Research Center and, in part, by gifts from E. I. duPont deNemours & Co. and ICI Composites.

where C_3 is a constant defined in the appendix, t_1 is the semi-thickness of the 90° plies and $\sigma_{x0}^{(1)}$ is the tensile stress in the 90° plies in the absence of microcracks: †

$$\sigma_{x0}^{(1)} = k_m^{(1)}\sigma_0 + k_{th}^{(1)}T \tag{2}$$

The terms $k_m^{(1)}$ and $k_{th}^{(1)}$ are the effective thermal and mechanical stiffnesses of the 90° plies. T is the temperature difference between the specimen temperature and the stress free temperature and it is used to define the level of residual thermal stresses in the specimen. By a simple one-dimensional, constant-strain analysis the stiffness constants are

$$k_m^{(1)} = \frac{E_x^{(1)}}{E_c^0} \qquad \text{and} \qquad k_{th}^{(1)} = -\frac{\Delta\alpha}{C_1} \tag{3}$$

Here E_c^0 is the x-direction modulus of the laminate, $E_x^{(1)}$ is the x-direction modulus of the 90° plies, $\Delta\alpha = \alpha_x^{(1)} - \alpha_x^{(2)}$ is the difference between the x-direction thermal expansion coefficients of the 90° plies and the (S) sublaminate, and C_1 is a constant defined in the appendix.

To use Eq. (1), $Y(D)$ is needed. Following Laws and Dvorak [22], Nairn *et. al.* [16, 19] evaluated $Y(D)$ for the discrete process of forming a new microcrack between two existing microcracks. The result is

$$Y(D) = \chi(\rho_k - \delta) + \chi(\delta) - \chi(\rho_k) \tag{4}$$

where $\chi(\rho)$ is a function defined in the appendix, $2\rho_k$ is the dimensionless distance between the existing microcracks, and 2δ is the dimensionless distance from the new microcrack to one of the existing microcracks [16, 19]. Normally one does not know where the next microcrack will form and therefore does not know ρ_k or δ. It is known, however, that $[(S)/90_n]_s$ laminates tend to form roughly periodic microcracks. We thus expect $\rho_k \approx \langle\rho\rangle$ and $\delta \approx \frac{\langle\rho\rangle}{2}$. Liu and Nairn [16], however, point out that these approximations are an oversimplification. From Eq. (1) it can be shown that the energy release rate is higher when the microcrack forms in a large microcrack interval than it is when it forms in a small microcrack interval. It is logical to assume that microcrack formation prefers the location that maximizes energy release rate. Thus when there is a distribution in crack spacings, the next microcrack will prefer to form in a crack interval that is larger than the average crack spacing. Liu and Nairn [16] introduced a factor f, defined as the average ratio of the crack spacing where the new microcrack forms to the average crack spacing. In this model, $Y(D)$ is approximated by

$$Y(D) \approx 2\chi(f\langle\rho\rangle/2) - \chi(f\langle\rho\rangle) \tag{5}$$

Using f values between 1.0 and 1.44, Liu and Nairn [16] get good fits to experimental results for a wide variety of laminates. Fortunately, the value of f required to get the best fit does not influence the calculated fracture toughness, G_{mc}. In this paper, we treat f as a layup independent factor that is approximately 1.2. There are tedious experimental techniques that can measure f and they show that it is usually about 1.2.

To predict microcracking results in $[90_n/(S)]_s$ laminates, Nairn and Hu [17] extended the variational analysis of $[(S)/90_n]_s$ laminates to account for the development of staggered microcracks. The analysis is more complicated due to the loss of symmetry resulting from staggered microcracks. Their results, however, can be cast in a form similar to the $[(S)/90_n]_s$ laminate results. The total strain energy release rate associated with an increase in microcracking damage is

$$G_m = \sigma_{x0}^{(1)2} C_{3a} t_1 Y_a(D) \tag{6}$$

† Note that Refs. [16, 17, 19–21] define $\sigma_{x0}^{(1)} = k_m^{(1)}\sigma_0$ or as the mechanical load in 90° plies of the undamaged laminate. As expressed in Eq. (2), we altered the definition of $\sigma_{x0}^{(1)}$ to also include the initial thermal stresses.

where C_{3a} is a constant defined in the appendix and $Y_a(D)$ can be approximated by [17]

$$Y_a(D) \approx \frac{1}{2}(3\chi_a(f\langle\rho\rangle/3) - \chi_a(f\langle\rho\rangle)) \tag{7}$$

Here, $\chi_a(\rho)$, which is given in the appendix, is the antisymmetric damage state analog of $\chi(\rho)$.

In this paper we describe the use of the above microcracking analyses to predict microcracking in 18 different layups of AS4/3501-6 laminates at room temperature and to predict the temperature dependence of microcracking in two different layups of AS4/PEEK laminates. In brief, the variational analysis was used to develop scaling laws that permit plotting the results from all laminates of a given material on a single linear master plot. The accuracy with which the experimental data conforms to the linear master plot predictions quickly reveals the adequacy of the analysis. Our findings were that the variational stress analysis coupled with an energy release rate failure criterion can predict all experimental results. All attempts at using simpler theories based on stress analyses that ignore the z dependence of the problem gave poor results.

MATERIALS AND METHODS

Static tensile tests were run on Hercules AS4 carbon fiber/3501-6 epoxy matrix composites and on Hercules AS4 carbon fiber/ICI Polyether ether ketone (PEEK) composites. AS4/3501-6 prepreg was purchased from Hercules and cured in an autoclave at 177°C according to manufacturer's recommendations. We made eight cross-ply layups with 90° plies in the middle—$[0/90]_s$, $[0/90_2]_s$, $[0/90_4]_s$, $[0_2/90]_s$, $[0_2/90_2]_s$, $[0_2/90_4]_s$, $[\pm 15/90_2]_s$, and $[\pm 30/90_2]_s$. We made 10 cross-ply layups with surface 90° plies—$[90/0/90]_T$, $[90/0]_s$, $[90/0_2]_s$, $[90/0_4]_s$, $[90_2/0/90_2]_T$, $[90_2/0]_s$, $[90_2/0_2]_s$, $[90_2/0_4]_s$, $[90_2/\pm 15]_s$, and $[90_2/\pm 30]_s$. Two cross-ply layups of AS4/PEEK composites—$[90_4/0_2]_s$ and $[90_4/0]_s$—were supplied by ICI Composites. Specimens, which were nominally 12 mm wide and 150 mm long with thicknesses determined by the stacking sequences (about 0.125 mm per ply), were cut from the laminate plates. Tensile tests were run in displacement control, at a rate of 0.005 mm/sec, on a Minnesota Testing Systems (MTS) 25 kN servohydraulic testing frame. While testing each specimen, the experiment was periodically stopped and the specimen was examined by optical microscopy. For $[(S)/90_n]_s$ laminates we calculated the crack density by averaging the densities of the cracks visible on the two specimen edges. For $[90_n/(S)]_s$ laminates, microcracks could be seen on the edges and on the faces of the specimen. We calculated the crack density by averaging the crack densities of the two 90° ply groups.

MASTER PLOT ANALYSIS

Assuming that microcracking occurs when $G_m = G_{mc}$, solving Eq. (1) for σ_0, and multiplying the result by $-k_m^{(1)}/k_{th}^{(1)}$ gives

$$-\frac{k_m^{(1)}}{k_{th}^{(1)}}\sigma_0 = -\frac{1}{k_{th}^{(1)}}\sqrt{\frac{G_{mc}}{C_3 t_1 Y(D)}} + T \tag{8}$$

A similar treatment of Eq. (6) yields an identical result except that C_{3a} and $Y_a(D)$ replace C_3 and $Y(D)$. These results lead us to define a reduced stress and a reduced crack density as

$$\begin{aligned}
&\text{reduced stress:} && \sigma_R &&= -\frac{k_m^{(1)}}{k_{th}^{(1)}}\sigma_0 \\
&\text{reduced crack density in } [(S)/90_n]_s \text{ laminates:} && D_R &&= -\frac{1}{k_{th}^{(1)}}\sqrt{\frac{1}{C_3 t_1 Y(D)}} \\
&\text{reduced crack density in } [90_n/(S)]_s \text{ laminates:} && D_R &&= -\frac{1}{k_{th}^{(1)}}\sqrt{\frac{1}{C_{3a} t_1 Y_a(D)}}
\end{aligned} \tag{9}$$

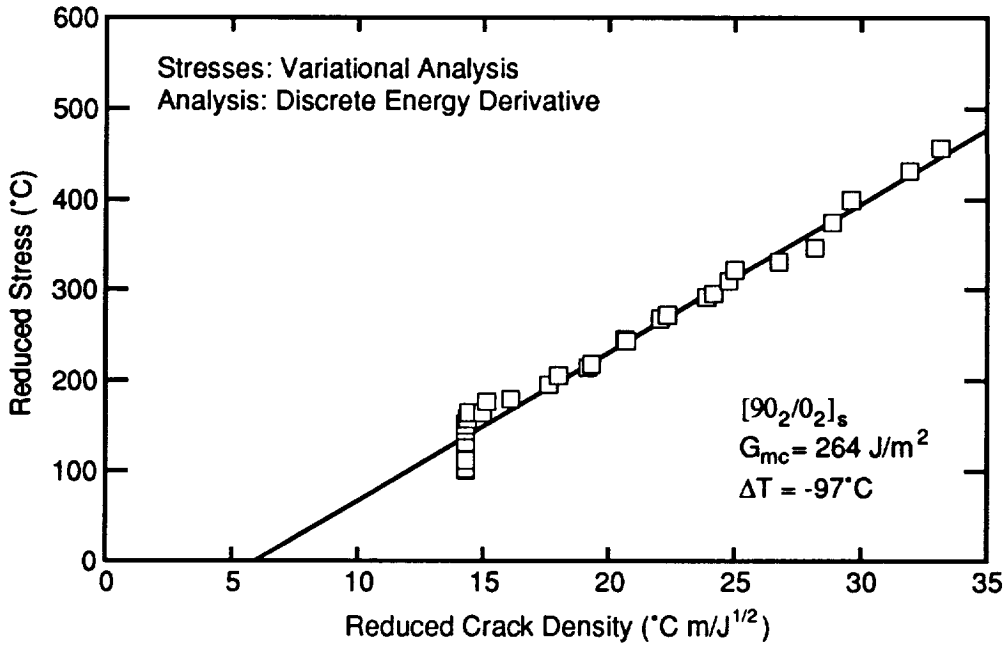

Figure 1: A master curve analysis of a $[90_2/0_2]_s$ AS4/3501-6 laminate. The energy release rate is calculated with a discrete energy derivative defined by $Y_a(D)$ in Eq. (7) using $f = 1.2$.

A plot of σ_R *vs.* D_R defines a master plot for microcracking experiments. If the variational analysis and energy release rate failure criterion are appropriate, a plot of σ_R *vs.* D_R will be linear with slope $\sqrt{G_{mc}}$ and intercept T. Because G_{mc} and T are layup independent material properties, the results from all laminates of a single material with the same processing conditions should fall on the same linear master plot.

A typical master curve analysis for a single $[90_2/0_2]_s$, AS4/3501-6 laminate is shown in Fig. 1. The master plot is linear except for a few points at the lowest crack density. The low crack density is believed to be caused by processing flaws that are not specifically included in the microcracking analysis [16]. They should be ignored when measuring G_{mc}. The straight line in Fig. 1 is the best linear fit that ignores the low crack density data. The slope gives $G_{mc} = 264$ J/m^2 which agrees with results in other studies [16]. The intercept gives $T = -93$°C. Note that a side benefit of the master curve analysis is that the value of T does not have to be assumed or measured. It can, in effect, be measured by analysis of the microcracking data.

Figure 2 gives the master plot for the 18 AS4/3501-6 laminates tested in this study. We assumed that $f = 1.2$ for all laminates and we ignored data with crack densities less than 0.3 mm^{-1}. We claim Fig. 2 verifies both the validity of an energy release rate failure criterion and the accuracy of the variational analysis calculation of G_m in Eqs. (1) and (6). There are three facts that support this claim. First, all laminates fall on a single master curve plot within a relatively narrow scatter band. The next paragraph discusses the scatter further. Second, the results for $[(S)/90_n]_s$ laminates (open symbols) agree with the results for $[90_n/(S)]_s$ laminates (solid symbols). Thus a single unified analysis can account for both the symmetric damage state in $[(S)/90_n]_s$ laminates and the antisymmetric damage state in $[90_n/(S)]_s$ laminates. Third, the slope and the intercept of the global linear fit in Fig. 2 result in $G_{mc} = 279$ J/m^2 and $T = -93$°C. Both of these results are reasonable measured values for these physical quantities.

There is an observable scatter band for the experimental points relative to the global, linear master curve. This scatter band may represent deficiencies in the analysis that need further refinement. Alternatively, we note that the scatter was caused more by a laminate to laminate variation in intercept than by a laminate to laminate variation in slope. It is thus possible that the scatter is due to real variations in T. Because all laminates were processed under identical conditions, T should be the same for all laminates. T, however, can also be interpreted as the *effective* level of residual thermal stresses. By

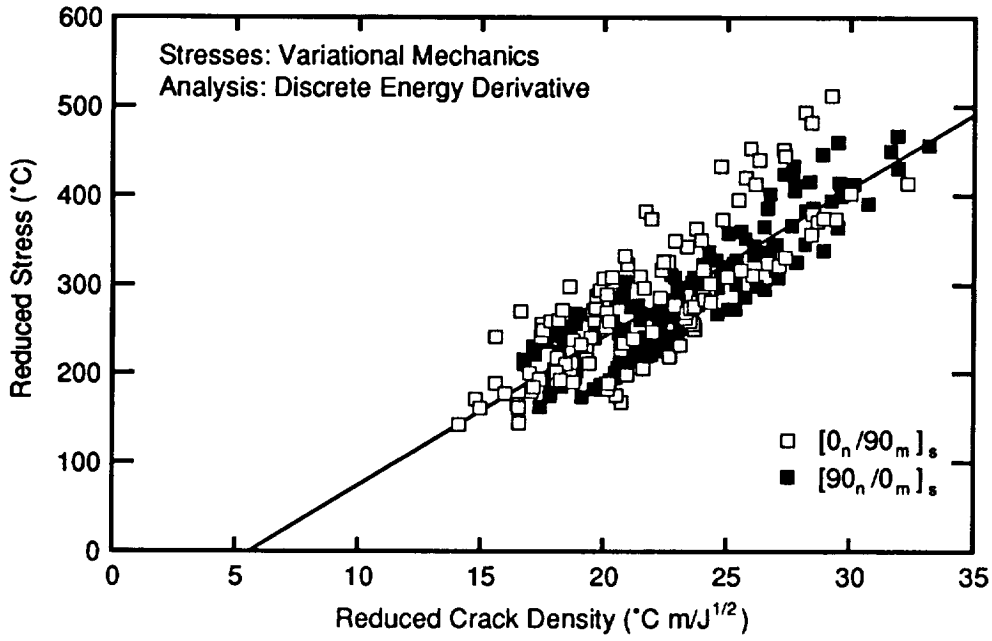

Figure 2: A master curve analysis of all AS4/3501-6 laminates. The energy release rate is calculated with a discrete energy derivative defined by $Y(D)$ or $Y_a(D)$ in Eqs. (5) and (7) using $f = 1.2$. Data for crack densities less than 0.3 mm^{-1} are not included in this plot.

Eq. (2), when $\sigma_0 = 0$ the residual stress in the 90° plies is $\sigma^{(1)}_{xx,th} = k^{(1)}_{th} T$. Although all laminates were processed under identical conditions, the laminates had different thicknesses. If the different thicknesses caused variations in thermal history, it is possible that the level of residual stresses was layup dependent. A layup dependence in T would cause the type of scatter observed in Fig. 2.

We turn next to the AS4/PEEK experiments. We tested two layups ($[90_4/0]_s$ and $[90_4/0_2]_s$) at three different temperatures (20°C, -10°C, and -50°C). Because we varied temperature, these results cannot be plotted on a single master plot. Both G_{mc} and T may be temperature dependent and thus data from different laminates would fall on lines with different slopes and intercepts. Some analyses of raw data, however, using the procedures in Refs. [16, 19] indicated that G_{mc} is independent of temperature or only weakly dependent on temperature in the range -50°C to 20°C. The major effect on the microcracking properties therefore arises from changes in the residual thermal stresses or in T. The room temperature experiments could be fit well with $T = -230$°C, which is similar to the $T = -250$°C used by Liu and Nairn [16]. Assuming linear thermoelasticity from -50°C to 20°C, T at -10°C and -50°C should be -260°C and -300°C, respectively. If we accept the previous values of T as reasonable measures of the residual thermal stresses in these laminates, and we assume G_{mc} is independent of temperature, we can propose a residual stress independent master plot. We redefine the reduced stress as

$$\text{modified reduced stress:} \quad \sigma'_R = -\frac{k^{(1)}_m}{k^{(1)}_{th}}\sigma_0 - T \tag{10}$$

A plot of σ'_R *vs.* D_R should be linear with a slope of $\sqrt{G_{mc}}$ and pass through the origin.

Figure 3 gives the master plot for the two AS4/PEEK laminates tested at each of the three test temperatures. We assumed that $f = 1.2$ for all laminates and we included data at all crack densities. The slope of the best fit line that is forced to pass through the origin gives $G_{mc} = 1500$ J/m^2. The experimental results conform reasonably well to the master line and the results from the different temperatures fall on the same line. Some of the scatter may be caused by temperature variations in G_{mc}, but we do not have enough data to prove or disprove this possibility. A master plot that ignores the change in residual thermal

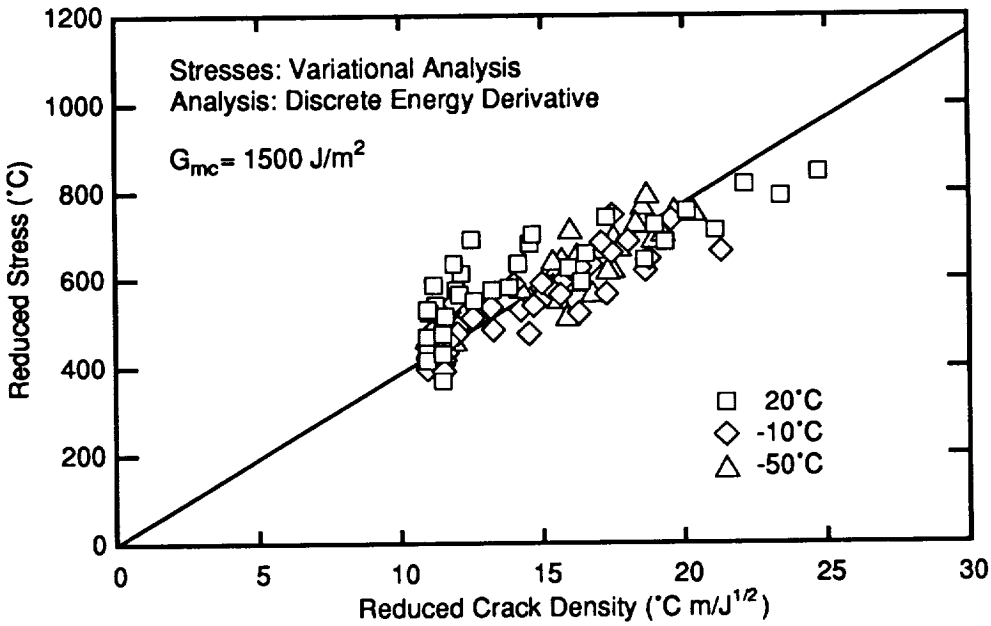

Figure 3: A master curve analysis of all AS4/PEEK laminates tested at 20°C, -10°C, and -50°C. The energy release rate is calculated with a discrete energy derivative defined by $Y(D)$ or $Y_a(D)$ in Eqs. (5) and (7) using $f = 1.2$.

stresses has two to three times the amount of scatter of the master plot in Fig. 3. These experiments thus demonstrate the real effect that residual thermal stresses have on microcracking properties of laminates. Finally, we note that previous attempts at studying microcracking in AS4/PEEK laminates used $[(S)/90_n]_s$ layups. The experiments showed only a few microcracks and yielded only a rough estimate of G_{mc} [17]. In this study the 90° plies were on the free surface instead of in the middle. The free-surface plies crack easier and we were thus able to get more experimental results and a more precise determination of G_{mc}. We recommend using $[90_n/(S)]_s$ laminates when studying microcracking in laminates with tough matrices.

OTHER MICROCRACKING THEORIES

Most previous microcracking theories are based on stress analyses that eliminate the z-dependence of the stress state by making various assumptions about the z-direction stress or displacement. The common assumptions are zero stress, zero average stress, or zero displacement. We classify any analysis using one of these assumptions as a "one-dimensional" analysis. Examples can be found in Refs. [1, 2, 5, 11, 22–30]. We note that some authors describe their analyses as "two-dimensional" analyses [25, 26, 29, 30]. In all cases, however, the second dimension is the y-dimension whose inclusion is little more than a marginal correction for Poisson's contraction. In this section we derive master plot methods from previous literature microcracking theories and use them to analyze our AS4/3501-6 experimental results.

Garrett and Bailey [1] postulated that the next microcrack forms when the maximum stress in the 90° plies reaches the transverse strength of those plies. Using their one-dimensional, shear-lag analysis, this model yields a linear master plot defined by

$$-\frac{k_m^{(1)}}{k_{th}^{(1)}}\sigma_0 = -\frac{1}{k_{th}^{(1)}}\frac{\sigma_T}{\left(1-\frac{1}{\cosh\Phi\rho}\right)} + T \tag{11}$$

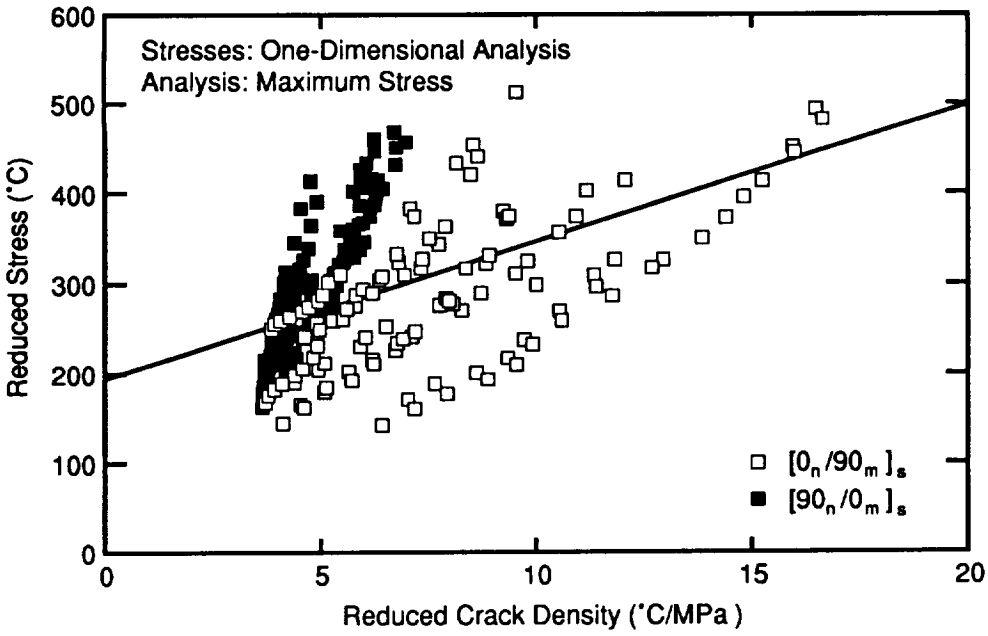

Figure 4: A master curve analysis of all AS4/3501-6 laminates using a maximum stress failure criterion and a one-dimensional stress analysis. Data for crack densities less than 0.3 mm^{-1} are not included in this plot.

where σ_T is the transverse strength of the 90° plies and $\Phi = \sqrt{G_{xz}^{(1)} C_1}$. Defining the reduced stress as in Eq. (9) and the reduced crack density as

$$\text{reduced crack density :} \qquad D_R = -\frac{1}{k_{th}^{(1)}} \frac{1}{\left(1 - \frac{1}{\cosh \Phi \rho}\right)}, \tag{12}$$

and using a master curve analysis, Eq. (11) predicts that a plot of σ_R *vs.* D_R should be linear with slope σ_T and intercept T.

The result of a strength theory analysis applied to our AS4/3501-6 experimental results is in Fig. 4. The master curve analysis shows the theory to be very poor. The results from individual laminates are somewhat nonlinear and they do not overlap the results from other laminates. Furthermore, the results from $[(S)/90_n]_s$ (open symbols) and $[90_n/(S)]_s$ (filled symbols) laminates segregate into two groups. This segregation is a characteristic of all one-dimensional analyses. Any analysis that ignores the z-dependence of the stress state will fail to make a distinction between inner and outer 90° ply groups. We therefore conclude that no model based on a one-dimensional stress analysis can successfully predict results for both $[(S)/90_n]_s$ and $[90_n/(S)]_s$ laminates. If we draw a least-squares linear fit through the data in Fig. 4, the slope and intercept give $\sigma_T = 15.2$ MPa and $T = +192°C$. These results are unreasonable because the transverse tensile strength of AS4/3501-6 laminates is higher than 15.2 MPa and T must be below zero for laminates that were cooled after processing.

Because of the problems with all strength analyses, numerous authors have suggested energy failure criteria for predicting microcracking [3, 5, 13, 14, 16, 17, 19, ?, 27, 28, 30]. Caslini *et. al.* [14] used a one-dimensional stress analysis that assumes parabolic displacements in the 90° plies [23, 24] to express the structural modulus as a function of crack density. They treated crack area, $A = 2t_1WLD$, as a continuous variable and differentiated the modulus expression to find energy release rate. Because they take an analytical derivative as a function of crack area, we refer to this approach as the "analytical derivative approach." By treating Eq. (1) as a definition of $Y(D)$, the Caslini *et. al.* [14] result for G_m can be

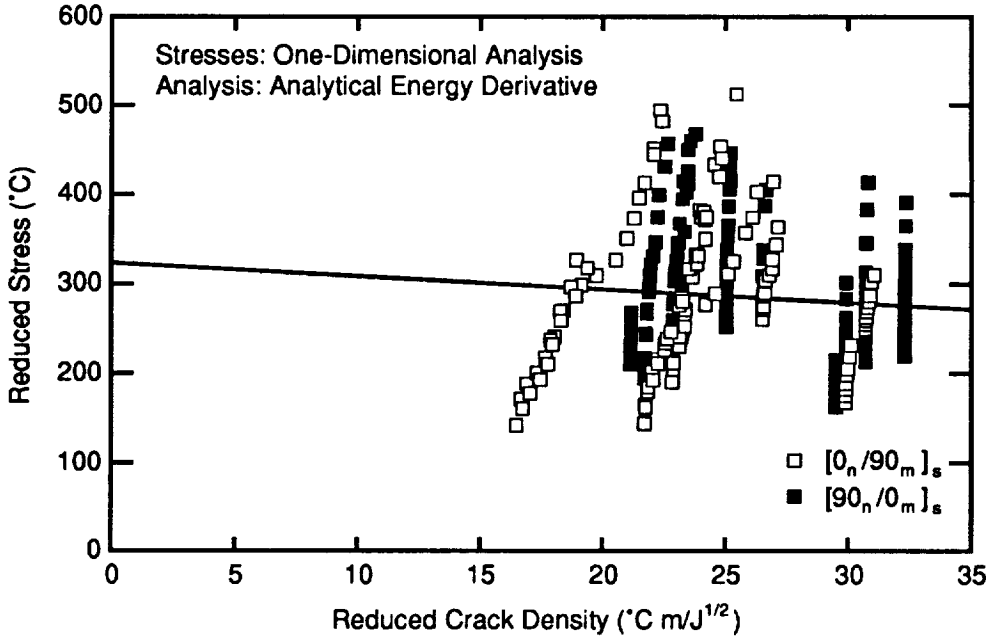

Figure 5: A master curve analysis of all AS4/3501-6 laminates using an analytical derivative energy release rate failure criterion and a one-dimensional stress analysis. Data for crack densities less than 0.3 mm^{-1} are not included in this plot.

expressed using

$$Y_{1D,a}(D) = \frac{C_1}{C_3\Phi}\left(\tanh\Phi\rho - \Phi\rho\,\mathrm{sech}^2\Phi\rho\right) \tag{13}$$

where subscript "$1D, a$" denotes one-dimensional stress analysis and an analytical derivative approach, and $\Phi = \sqrt{3G_{xz}^{(1)}C_1}$. Han *et. al.* [27, 28] describe a similar analysis based on crack closure that gives the same G_m. Their approach is thus also an analytical derivative model.

By replacing $Y(D)$ and $Y_a(D)$ with $Y_{1D,a}(D)$ we can evaluate the microcracking models in Refs. [14, 27, 28]. The results of such an analysis applied to our AS4/3501-6 experimental results are in Fig. 5. This master curve analysis was the worst of any model we evaluated. The results from individual laminates are fairly linear but they give slopes and intercepts corresponding to toughnesses as high as 10^{12} J/m^2 and T's that imply specimen temperatures well below absolute zero. These are clearly unreasonable results. The least-squares linear fit through the data in Fig. 5 gives $G_{mc} = 2$ J/m^2 and $T = +323$°C, both of which are unrealistic.

In the *Master Plot Analysis* section, we argued that microcracking should be analyzed using energy release rate methods. We are left with explaining why the analytical derivative approach is a complete failure. Our first attempt was to use the variational mechanics stress analysis and calculate G_m by a similar analytical derivative approach. This made slight improvements in the master curve but the overall quality and the fitting constants were still unsatisfactory. We suggest instead that the analytical derivative approach is non-physical and therefore $Y_{1D,a}(D)$ gives the *wrong* energy release rate. The analytical derivative energy release rate at a given crack density corresponds to the unlikely fracture event whereby all cracks close and then reopen again as periodic cracks with a slightly higher crack density. In real microcracking, one microcrack forms between two existing microcracks. Apparently the energy release rate for this process is dramatically different from the one calculated with an analytical derivative.

Laws and Dvorak [22] were the first to suggest modelling the actual fracture process. They calculated the change in energy associated with the formation of a new microcrack between two existing microcracks. Because they model a discrete process, we call their approach the "discrete derivative approach." We can

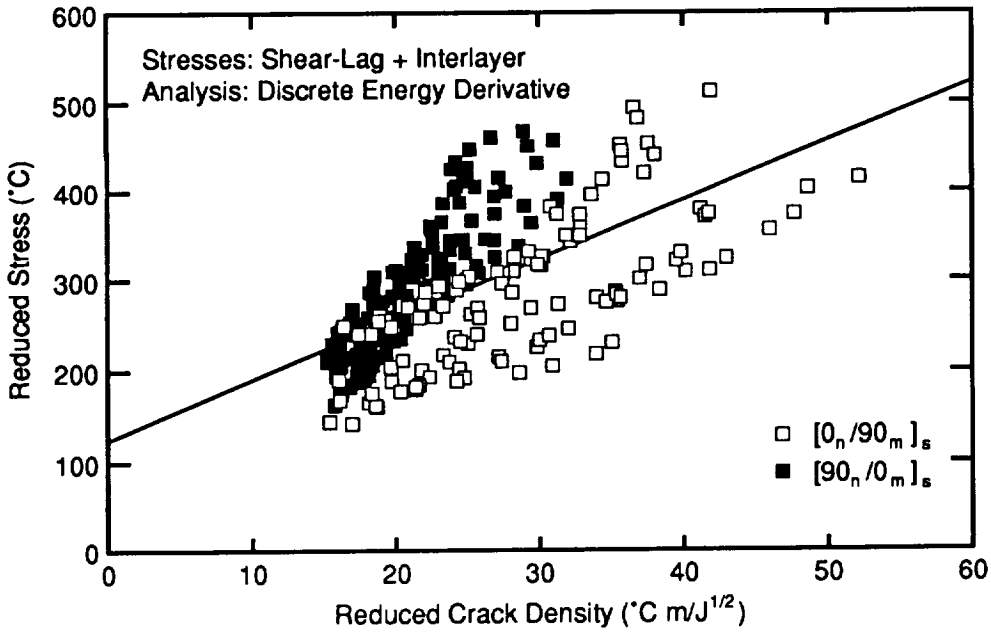

Figure 6: A master curve analysis of all AS4/3501-6 laminates using a discrete derivative energy release rate failure criterion and a one-dimensional stress analysis. Data for crack densities less than 0.3 mm^{-1} are not included in this plot.

cast Laws and Dvorak's [22] result in the form of the variational analysis by redefining $Y(D)$ to be

$$Y_{1D,d}(D) = \frac{C_1}{C_3\Phi}\left(2\tanh f\Phi\rho/2 - \tanh f\Phi\rho\right) \tag{14}$$

where subscript "$1D, d$" denotes one-dimensional stress analysis and a discrete derivative approach, and f is the factor introduced earlier to account for the tendency of microcracks to prefer larger than average microcrack intervals. Following Reifsnider [2], Laws and Dvorak [22] used a shear-lag analysis that assumes an interlayer of unknown thickness and stiffness between the (S) sublaminate and the 90° plies. Their Φ can be expressed as

$$\Phi = \sqrt{\frac{Gt_1C_1}{t_0}} \tag{15}$$

where G is the shear modulus of the interlayer and t_0 is its thickness.

By replacing $Y(D)$ and $Y_a(D)$ with $Y_{1D,d}(D)$ we can evaluate the Laws and Dvorak [22] microcracking model. A drawback of their analysis is that the effective stiffness of the interlayer is an unknown parameter. Laws and Dvorak [22] suggested a circular scheme in which G/t_0 is determined by prior knowledge of G_{mc} and the stress required to form the first microcrack. Because of our concern about the sensitivity of low crack density results to laminate processing flaws, we instead used the high crack density results from the single laminate in Fig. 1 to determine G/t_0. We varied G/t_0 until the slope of the Laws and Dvorak [22] analysis master curve gave G_{mc} equal to the variational analysis result of 280 J/m^2. This exercise yielded $G/t_0 = 4000$ N/mm, a linear master curve, and an intercept of $T = -73°C$. These initial results were promising. The results of a master plot analysis applied to our AS4/3501-6 experimental results using $Y_{1D,d}(D)$, $G/t_0 = 4000$ N/mm, and $f \approx 1.2$ are in Fig. 6. This master curve analysis is the most satisfactory of all previous literature models but it still has serious problems. Most importantly, the results from individual lamina do not overlap each other. As is characteristic of one-dimensional analyses, the results from $[(S)/90_n]_s$ and $[90_n/(S)]_s$ laminates segregate into two groups. The least-squares linear fit through the data in Fig. 6 gives $G_{mc} = 44$ J/m^2 and $T = +124°C$, both of which are unrealistic.

We believe the only problem with the Laws and Dvorak [22] analysis is its use of an oversimplified, one-dimensional stress analysis. If their failure criterion is implemented with the variational mechanics stress analysis, the result is equivalent to the analysis first presented by Nairn [19]. As shown in the *Master Plot Analysis* section, such an analysis gives a good master plot (see Fig. 2).

CONCLUSIONS

All analyses of composite failure can be divided into at least two separate parts. First, failure analyses must solve for the stresses in the presence of damage. These stress analyses will normally involve some simplifying assumptions. Second, to predict failure, it is necessary to assume some sort of failure criterion. The master plot analysis of microcracking shows that both the stress analysis and the failure criterion must be appropriate to be able to predict experimental results.

We considered first the stress analysis part of a failure model. Our master plot analyses in Figs. 2–3 used a two-dimensional, variational mechanics stress analysis. Such a stress analysis appears adequate for explaining microcracking. We tried numerous master plot analyses using one-dimensional stress analyses and all of them, regardless of failure criterion, gave poor results. We thus suggest that future attempts at predicting composite cracking abandon use of one-dimensional analyses and treat the variational analysis as a base-line stress analysis.

If one plots the stresses calculated by a one-dimensional analysis and those calculated by a variational analysis, the differences are marked, but hardly dramatic. We were thus initially surprised by the dramatic differences between the predictions based on the two analyses. A qualitative interpretation of the differences can follow from realizing that fracture is an instability event. When calculating instability processes, minor differences in input stresses can lead to dramatic differences in predictions. In other words, the increased accuracy in the stresses attributed to the variational analysis was crucial to the predictions of microcracking. In contrast, non-instability properties, such as plate stiffness or in-plane displacements, are much easier to predict. Researchers have been mislead into believing that one-dimensional analyses are reasonably accurate due to their ability to predict such non-instability properties.

Next, we considered the failure criterion. There is a disturbing tendency of composite failure analyses to concentrate on sophisticated stress analysis or involved finite element analysis and to give too little thought to choosing the most appropriate failure criterion. As a result, one often finds complex failure models that are based on simplistic failure criteria such as maximum stress, maximum strain, average stress, point stress, or quadratic stress functions. We found that all such simplistic failure criteria gave very poor results when used to predict composite microcracking. To get a successful master plot analysis we had to use a failure criterion based on energy release rate. We further had to find the energy release rate for the actual fracture process (the discrete derivative approach). Pseudo-energy release rates, such as the analytical derivative approach, that are not derived from a realistic fracture model, give the *wrong* energy release rate, and, not surprisingly, gave poor master plot results.

We claim that microcracking, in being controlled by energy release rate, is not a unique composite failure mechanism. Instead, energy release rate is a powerful technique that should be applicable to all composite failure mechanisms. We further suggest that because energy release rate is the fundamental failure criterion, that composite failure models couched in stress-based failure criteria are doomed to inadequacy unless it can be demonstrated mathematically that the stress failure criterion is equivalent to an energy release rate criterion. A similar situation exists in the fracture of isotropic, homogeneous materials where a stress criterion or critical stress intensity factor can predict failure because it is exactly related to energy release rate. No one would consider using maximum stress, maximum strain, average stress, point stress, or quadratic stress functions to predict failure in cracked isotropic, homogeneous materials. Likewise, no one should consider using such failure criteria in composite materials.

REFERENCES

1. Garrett, K. W.; and Bailey, J. E.: Multiple Transverse Fracture in 90° Cross-Ply Laminates of a Glass Fibre-Reinforced Polyester. *J. Mat. Sci.*, vol. 12, 1977, pp. 157–168.
2. Reifsnider, K. L.: Some Fundamental Aspects of the Fatigue and Fracture Response of Composite Materials. *Proc. 14th Annual Meeting of SES, Lehigh, PA, November*, 1977, pp. 373–383.
3. Parvizi, A.; Garrett, K. W.; and Bailey, J. E.: Constrained Cracking in Glass Fiber-Reinforced Epoxy Cross-Ply Laminates. *J. Mat. Sci.*, vol. 13, 1978, pp. 195–201.
4. Parvizi, A.; and Bailey, J. E.: On Multiple Transverse Cracking in Glass-Fiber Epoxy Cross-Ply Laminates. *J. Mat. Sci.*, vol. 13, 1978, pp. 2131–2136.
5. Bailey, J. E.; Curtis, P. T.; and Parvizi, A.: On the Trans. Cracking and Long. Splitting Behavior of Glass and Carbon Fibre Epoxy X-Ply Laminates and the Effect of Poisson and Thermally Generated Strains. *Proc. R. Soc. Lond. A*, vol. 366, 1979, pp. 599–623.
6. Bader, M. G.; Bailey. J. E.; Curtis, P. T.; and Parvizi, A.: The Mechanisms of Initiation and Development of Damage in Multi-Axial Fibre-Reinforced Plastics Laminates. *Proc. 3rd Int'l Conf. on Mechanical Behavior of Materials*, vol. 3, 1979, pp. 227–239.
7. Stinchcomb, W. W.; Reifsnider, K. L.; Yeung, P.; and Masters, J.: Effect of Ply Constraint on Fatigue Damage Development in Composite Material Laminates. *ASTM STP*, vol. 723, 1981, pp. 64–84.
8. Flaggs, D. L.; and Kural, M. H.: Experimental Determination of the In Situ Transverse Lamina Strength in Graphite/Epoxy Laminates. *J. Comp. Mat.*, vol. 16, 1982, pp. 103–115.
9. Crossman, F. W.; and Wang, A. S. D.: The Dependence of Transverse Cracking and Delamination on Ply Thickness in Graphite/Epoxy Laminates. *ASTM STP*, vol. 775, 1982, pp. 118–139.
10. Highsmith, A. L.; and Reifsnider, K. L.: Stiffness-Reduction Mechanisms in Composite Laminates. *ASTM STP*, vol. 775, 1982, pp. 103–117.
11. Manders, P. W.; Chou, T, W,; Jones, F. R.; and Rock, J. W.: Statistical Analysis of Multiple Fracture in [0/90/0] Glass fiber/epoxy resin laminates. *J. Mat. Sci.*, vol. 19, 1983, pp. 2876–2889.
12. Peters, P.W.M.: The Strength Distribution of 90° Plies in 0/90/0 Graphite-Epoxy Laminates. *J. Comp. Mat.*, vol. 18, 1984, pp. 545–556.
13. Wang, A. S. D.; Kishore, N. N.; and Li, C. A.: Crack Development in Graphite-Epoxy Cross-Ply Laminates under Uniaxial Tension. *Comp. Sci. & Tech.*, vol. 24, 1985, pp. 1–31.
14. Caslini, M.; Zanotti, C.; and O'Brien, T. K.: Fracture Mechanics of Matrix Cracking and Delamination in Glass/Epoxy Laminates. *J. Comp. Tech & Research*, vol. Winter, 1987, pp. 121–132. (Also appeared as NASA TM89007, 1986).
15. Groves, S. E.; Harris, C. E. ; Highsmith, A. L.; and Norvell, R. G.: An Experimental and Analytical Treatment of Matrix Cracking in Cross-Ply Laminates. *Experimental Mechanics*, vol. March, 1987, pp. 73–79.
16. Liu, S.; and Nairn, J. A.: The Formation and Propagation of Matrix Microcracks in Cross-Ply Laminates During Static Loading. *J. Reinf. Plast. & Comp.*, vol. 11, 1992, pp. 158–178.
17. Nairn, J. A.; and Hu, S.: The Formation and Effect of Outer-Ply Microcracks in Cross-Ply Laminates: A Variational Approach. *Eng. Fract. Mech.*, vol. 41, 1992, pp. 203–221.
18. Bowles, D. E.: Effect of Microcracks on the Thermal Expansion of Composite Laminates. *J. Comp. Mat.*, vol. 17, 1984, pp. 173–187.
19. Nairn, J. A.: The Strain Energy Release Rate of Composite Microcracking: A Variational Approach. *J. Comp. Mat.*, vol. 23, 1989, pp. 1106–1129. (See *errata*: *J. Comp. Mat.*, vol. 24, 1990, pp. 233–234).
20. Hashin, Z.: Analysis of Cracked Laminates: A Variational Approach. *Mech. of Mat.*, vol. 4, 1985, pp. 121–136.
21. Hashin, Z.: Analysis of Stiffness Reduction of Cracked Cross-Ply Laminates. *Eng. Fract. Mech.*, vol. 25, 1986, pp. 771–778.

22. Laws, N.; and Dvorak, G. J.: Progressive Transverse Cracking in Composite Laminates. *J. Comp. Mat.*, vol. 22, 1988, pp. 900–916.
23. Ogin, S. L.; Smith, P. A.; and Beaumont, P. W. R.: Matrix Cracking and Stiffness Reduction during the Fatigue of a $(0/90)_s$ GFRP Laminate. *Comp. Sci. & Tech.*, vol. 22, 1985, pp. 23–31.
24. Ogin, S. L.; Smith, P. A.; and Beaumont, P. W. R.: A Stress Intensity Approach to the Fatigue Growth of Transverse Ply Cracks. *Comp. Sci. & Tech*, vol. 24, 1985, pp. 47–59.
25. Flaggs, D. L.: Prediction of Tensile Matrix Failure in Composite Laminates. *J. Comp. Mat.*, vol. 19, 1985, pp. 29–50.
26. Fukunaga, H.; Chou, T. W.; Peters, P. W. M.; and Schulte, K.: Probabilistic Failure Strength Analysis of Graphite/Epoxy Cross-Ply Laminates. *J. Comp. Mat.*, vol. 18, 1984, pp. 339–356.
27. Han, Y. M.; Hahn, H. T.; and Croman, R. B.: A Simplified Analysis of Transverse Ply Cracking in Cross-Ply Laminates. *Proc. Amer. Soc. of Comp., 2^{nd} Tech. Conf.*, 1987, pp. 503–514.
28. Han, Y. M.; Hahn, H. T.; and Croman, R. B.: A Simplified Analysis of Transverse Ply Cracking in Cross-Ply Laminates. *Comp. Sci. & Tech.*, vol. 31, 1988, pp. 165–177.
29. Nuismer, R. J.; and Tan, S. C.: Constitutive Relations of a Cracked Composite Lamina. *J. Comp. Mat.*, vol. 22, 1988, pp. 306–321.
30. Tan, S. C.; and Nuismer, R. J.: A Theory for Progressive Matrix Cracking in Composite Laminates. *J. Comp. Mat.*, vol. 23, 1989, pp. 1029–1047.

APPENDIX

In the variational mechanics analysis of $[(S)/90_n]_s$ laminates [16, 19–21] we define the following constants:

$$C_1 = \frac{1}{E_x^{(1)}} + \frac{1}{\lambda E_x^{(2)}} \tag{16}$$

$$C_2 = \frac{\nu_{xz}^{(1)}}{E_x^{(1)}}\left(\lambda + \frac{2}{3}\right) - \frac{\lambda \nu_{xz}^{(2)}}{3E_x^{(2)}} \tag{17}$$

$$C_3 = \frac{1}{60E_z^{(1)}}\left(15\lambda^2 + 20\lambda + 8\right) + \frac{\lambda^3}{20E_z^{(2)}} \tag{18}$$

$$C_4 = \frac{1}{3G_{xz}^{(1)}} + \frac{\lambda}{3G_{xz}^{(2)}} \tag{19}$$

where $E_x^{(i)}$ and $E_z^{(i)}$ are the x- and z-direction moduli of ply group i, $G_{xz}^{(i)}$ is the $x-z$ plane shear modulus of ply group i, and $\lambda = t_1/t_2$. Superscripts (1) and (2) denote properties of the 90° plies and the (S) sublaminate, respectively. t_1 and t_2 are the ply thicknesses of the 90° and 0° ply groups. Defining $p = \frac{C_2 - C_4}{C_3}$ and $q = \frac{C_1}{C_3}$ there are two forms for the function $\chi(\rho)$. When $4q/p^2 > 1$

$$\chi(\rho) = 2\alpha\beta(\alpha^2 + \beta^2)\frac{\cosh 2\alpha\rho - \cos 2\beta\rho}{\beta \sinh 2\alpha\rho - \alpha \sin 2\beta\rho} \tag{20}$$

where

$$\alpha = \frac{1}{2}\sqrt{2\sqrt{q} - p} \qquad \text{and} \qquad \beta = \frac{1}{2}\sqrt{2\sqrt{q} + p} \tag{21}$$

When $4q/p^2 < 1$

$$\chi(\rho) = \alpha\beta(\beta^2 - \alpha^2)\frac{\tanh \alpha\rho \tanh \beta\rho}{\beta \tanh \beta\rho - \alpha \tanh \alpha\rho} \tag{22}$$

where

$$\alpha = \sqrt{-\frac{p}{2} + \sqrt{\frac{p^2}{4} - q}} \qquad \text{and} \qquad \beta = \sqrt{-\frac{p}{2} - \sqrt{\frac{p^2}{4} - q}} \tag{23}$$

In the variational mechanics analysis of $[90_n/(S)]_s$ laminates [17] we define some new constants:

$$C_{2a} = -\frac{\nu_{xz}^{(1)}}{3E_x^{(1)}} + \frac{\nu_{xz}^{(2)}}{E_x^{(2)}}\left(1 + \frac{2\lambda}{3}\right) \tag{24}$$

$$C_{3a} = \frac{1}{20E_z^{(1)}} + \frac{\lambda}{60E_z^{(2)}}\left(8\lambda^2 + 20\lambda + 15\right) \tag{25}$$

$$C_1^* = \frac{1}{E_x^{(1)}} + \frac{(1+2\lambda)^2}{\lambda^3 E_x^{(2)}} \tag{26}$$

$$C_2^* = -\frac{\nu_{xz}^{(1)}}{3E_x^{(1)}} + \frac{\nu_{xz}^{(2)}}{E_x^{(2)}}\left[\frac{(1+2\lambda)(2+\lambda)}{3\lambda}\right] \tag{27}$$

$$C_3^* = \frac{1}{20E_z^{(1)}} + \frac{\lambda}{60E_z^{(2)}}\left(2\lambda^2 + 7\lambda + 8\right) \tag{28}$$

$$C_4^* = \frac{1}{3G_{xz}^{(1)}} + \frac{1+\lambda+\lambda^2}{3\lambda G_{xz}^{(2)}} \tag{29}$$

The function $\chi_a(\rho)$ is expressed in terms of $\chi(\rho)$ and $\chi^*(\rho)$ as

$$\chi_a(\rho) = \frac{2\chi\left(\frac{\rho}{2}\right)}{1 + \frac{C_3\chi\left(\frac{\rho}{2}\right)}{C_3^*\chi^*\left(\frac{\rho}{2}\right)}} \tag{30}$$

where $\chi(\rho)$ is defined above except that we must redefine $p = \frac{C_{2a}-C_4}{C_{3a}}$ and $q = \frac{C_1}{C_{3a}}$. Defining $p^* = \frac{C_2^*-C_4^*}{C_3^*}$ and $q^* = \frac{C_1^*}{C_3^*}$, the new function $\chi^*(\rho)$ has two forms. When $4q^*/p^{*2} > 1$

$$\chi^*(\rho) = 2\alpha^*\beta^*\left(\alpha^{*2} + \beta^{*2}\right)\frac{\cosh 2\alpha^*\rho + \cos 2\beta^*\rho}{\beta^*\sinh 2\alpha^*\rho - \alpha^*\sin 2\beta^*\rho} \tag{31}$$

When $4q^*/p^{*2} < 1$

$$\chi^*(\rho) = \alpha^*\beta^*\left(\beta^{*2} - \alpha^{*2}\right)\frac{1}{\beta^*\tanh\alpha^*\rho - \alpha^*\tanh\beta^*\rho} \tag{32}$$

In the previous four equations, α^* and β^* are given by Eq. (21) and (23) with p and q replaced by p^* and q^*.